International Journal of GEOMATE, July., 2021, Vol.21, Issue 83, pp.-191-198
ISSN: 2186-2982 (P), 2186-2990 (O), Japan, DOI: https://doi.org/10.21660/2021.83.j2158
Geotechnique, Construction Materials and Environment

ESTIMATING ADDITIONAL FLOOD WARNING TIME USING RAINDROPS INTENSITY DATA CAPTURED BY X-BAND MP RADAR

*Adam Pamudji Rahardjo[1], Muhammad Anzhari Syahmi[2] and Djoko Legono[3]

[1,2,3] Faculty of Engineering , Universitas Gadjah Mada, Indonesia

*Corresponding Author, Received: 2 April 2021, Revised: 22 April 2021, Accepted: 3 May 2021

ABSTRACT: The current monitoring system of flood warnings on Mt. Merapi slope, Yogyakarta, Indonesia relies on rainfall gages and visual observation. Most flood events occurred with a fast-moving front resulting in a very short available warning time. An X-Band Multi-Parameter Radar installed at the southwest slope of Mt. Merapi measures raindrop intensity high above the ground and provides rainfall information earlier. This paper presents the effort to estimate the additional warning time available by extracting binary radar data, transforming it into 3D grid data, and visualize it into meaningful charts. This study compared the IDW and NN interpolation methods and verified the grid resolution and the limiting distance, *r*, of the IDW method for obtaining optimal performance. This study also conducted a qualitative review on the sequences of horizontal contour images and the comparison of horizontal and vertical grid resolutions. The estimation of time lag of peak raindrop intensity of different elevations was evaluated qualitatively by overlaying time-series data at four elevations and quantitatively by conducting a cross-correlation analysis of pairs of time series data of +3000 m and +1300 m elevations with horizontal offset for considering wind drift. The result shows that the optimal value of *r* is 400 m, and the optimal grid resolution is 100x100x100 m. It found that the approximate additional warning time was 6 minutes. The conclusion is that the developed interpolation method is reliable for raindrop analysis. The cross-correlation analysis gives a conservative estimate of the additional warning time.

Keywords: Flash flood warning, X-Band MP Radar data interpolation, Warning time, Cross-Correlation

1. INTRODUCTION

Flash floods frequently occurred on the slope of the Merapi volcano, located in the north tip of the Special Region of Yogyakarta, Indonesia, especially on the southwest side with higher heavy rainfall than those of the other sides [1]. After volcanic eruptions, flash floods carry debris from sand to boulder (Jumoyo, Gendol, and Krasak cases). Recently, on the 2nd of February 2020, a flash flood dragged down 257 junior secondary students, and 4 of them were dead (Sempor Creek, Turi District, Sleman Regency). Flood early warning is needed in this area to reduce the risk of loss of lives.

Several rainfall stations have been installed on the Merapi volcano slope area by the Hydrology and Hydraulics Laboratory of Civil and Environmental Department, Universitas Gadjah Mada, and the Sabo Engineering Unit of the Ministry of Public Works and Housing, Republic Indonesia, since ninety eighties. Within the last ten years, the laboratory installed more ground rainfall stations, but some of them were reduced their performance.

The network of rainfall gages may not detect a heavy local rainfall occurrence that causes a flash flood, because they do not drop exactly at the gage locations. In 2016, there has been installed a radar rainfall gauge on top of the roof of Mt. Merapi Museum building at the south-southwest of Merapi volcano slope. See the map in Fig. 1. This radar rainfall station was still under study. Several studies have used radar rainfall data, such as in [2–5]. However, the researchers and the other users have not utilized the 3D features of the recorded radar rainfall data extensively.

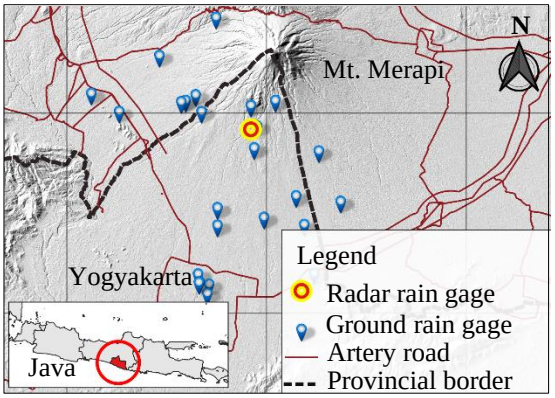

Fig.1 Location of the rainfall radar and ground station gauges

The purpose of this study is to develop a method that uses 3D radar rainfall data to estimate the delay time of radar rainfall data records of high elevation to reach the lowest elevation or the ground. By knowing this delay time, it is possible to lengthen the available flood warning time calculated from ground station rainfall data and the approximated flood travel time.

2. METHODS

2.1 Radar for Rainfall Measurement

The rainfall radar system installed in Merapi volcano slope is an X-Band Multi-Parameter Dual Polarimetry of WR-2100 Model produced by the Furuno Electric., Japan. The exact location of the radar antenna device is at 98° 27' 51" E, 3° 8' 27" S and the antenna altitude is at +1,257 m above mean sea level. Fig. 2 shows the radar dome installation and Table 1. shows the specification of the installed rainfall radar.

Fig.2 Installation of the MP DP X-Band Radar

This study uses rainfall intensity data, R (mm/hour), recorded in scan mode of Plan Position Indicator (PPI) with several tilt positions. Therefore, R data position is in an azimuth (degree) - tilt angle (degree) - range (m) coordinate system. Scanning setting of the radar provides R data on 968 azimuth data within 360°, 300 range data within 30 Km radius, and nine tilt data of 3°, 5°, 7°, 9°, 11°, 13°, 15°, 18°, and 21°. However, in the collected data, the azimuth intervals are not exactly equal to 360 divided by 968 but slightly shifted and vary tilt-to-tilt angels. One cycle of scanning that covers all tilt levels, takes about 2 minutes. The range data positions start from 100 m, followed by 200 m, 300 m, and so on, until 30,000 m. In such a data capture position system, the distance between two data locations on two adjacent rays of different azimuth values but with the same tilt angle and the same distance (range or radius) varies so much. For example, for the 3° tilt angle, the horizontal distance between two adjacent rays varies from 0.648 m to 194.460 m at 100 m to 30,000 m distance away from the radar antenna, respectively. In all vertical slices corresponding to azimuth values, the vertical distances between two adjacent arrays vary from 3.490 m to 1570.617 m at 100 m to 30,000 m distance away from the radar antenna, respectively.

Table 1. Specification of the MP DP X-Band Radar related to rainfall data[6]

Item	Specification
Polarization	Dual polarimetry (vertical and horizontal)
Operating Freq.	9470 MHz
Beam Width	2.7°
Hor. Scan Angle	360°
Ver. Scan Angle	-2^0 to 90^0
Angle Resolution	0.1°
Anten. Rot. Speed	0.5 to 16 rpm
Max. Range	30 Km

The above description shows that the ratio of the tangential distance, either vertically or horizontally, to the radial distance of neighbouring data locations on two adjacent rays varies so much. See Fig. 3. Throughout the measurement coverage area, the data locations are not in regular distances except along the rays. In such above irregularity of the rainfall data locations, it is difficult to do any numerical analysis (e.g. numerical weather prediction) directly using the PPI data. Therefore, interpolation to a regular grid is necessary.

2.2 Approximating R values in a regular grid

It is common to construct a CAPPI (constant altitude plan position indicator) and having data on a two-dimensional (2D) grid of a specific elevation [7, 8] or even in a 3D grid [9,10]. An interpolation technique may transform the PPI data to the CAPPI data or 3D grid data. Based on the 3D grid data, the R values at any position (e.g. in creating contours) can be obtained by using any grid-based interpolation method. Displaying the 3D data can apply any contouring technique on horizontal slices of several elevations (CAPPI) and vertical slices (VCUT). Visualization of 3D rainfall data helps observers to identify quickly any rainfall that is likely to produce a flash flood event. However, for

broad and deep observation areas, the closer contours may block those behind them.

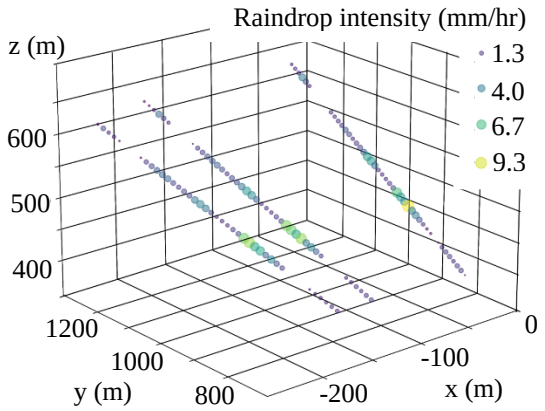

Fig. 3 An example of locations of R data along three adjacent rays

The recorded PPI rainfall data are in a .scn file (binary data format) for each tilt level along with other data and several parameters. The necessary data extraction method selects and takes the rainfall data of all azimuth and range values from the .scn file of a specific tilt level. The file name of the .scn file indicates the date, time, and tilt level.

2.3 CAPPI and 3D grid

Several methods for creating CAPPI data from the primary data (PPI) are available, such as the linear interpolation method that uses data on the neighbouring upper and lower rays, and data projection of rays to the CAPPI. Another method is an interpolation method that uses data at the neighbouring PPI with a distance criterion. This method does not create CAPPI data on grid nodes but directly on 2D contour lines/pixels at a certain altitude.

In WRADLIB [10], an open-source library specific for radar data processing, CAPPI data construction is done by data interpolation of the converted PPI data in Cartesian coordinate x, y, z to a 3D Cartesian grid. Based on the 3D grid, an instant of CAPPI can be created. There are several options of the interpolation methods to use, namely the nearest-neighbour method, the inverse distance method, the linear method, the ordinary kriging method, and the external drift kriging method. However, there is no explanation in detail of how far the maximum distance of the neighbouring PPI nodes whose values contribute to the interpolated value of a node in the 3D grid.

The single-pass isotropic Barnes distance-dependent weight method was used for mapping radar data from several weather radars with different types, namely the ARM scanning (C- and X-Band Radar) and the NEXRAD (S-Band Radar) data to a Cartesian grid of [11]. This method solves the problems of multi-radar systems that have different data systems.

2.4 Interpolation methods

This study verified the smoothness of the contour images resulted from two interpolation methods namely the Nearest Neighbour (NN) method and the Inverse Distance Weighting (IDW) method. The NN method takes the nearest available data point and neglects the values at other near data points. The IDW method computes the near available data points using the formula shown in Eq. (1).

$$R = \frac{\sum_{i=1}^{N} w_i(\mathbf{x})\, R_i}{\sum_{i=1}^{N} w_i(\mathbf{x})} \tag{1}$$

where,

$$w_i(\mathbf{x}) = \frac{1}{\|\mathbf{x}-\mathbf{x}_i\|^p}; \quad \|\mathbf{a}\| = \sqrt{a_1^2 + a_2^2 + a_3^2},$$

R is the interpolated value, R_i is the value at the ith available data point, $\mathbf{x}$ is the position vector of the interpolated data, $\mathbf{x}_i$ is the ith position vector of the ith available data point, $\mathbf{a}$ is the distance vector, $w_i(\mathbf{x})$ is the weighting coefficient of R_i, p is a power constant, and N is the number of the near data points. The near data points have the distance to the interpolated data point less than a selected limit.

2.5 Raindrops vertical movement

To approximate the time for raindrops traveling from their initial positions to the ground, a visual observation can examine a sequence of 2D vertical contour maps of raindrop intensity at a certain location while time elapses. If there is no horizontal movement of raindrops perpendicular to the 2D vertical contour map, two successive images of the vertical slice (VCUT) may show the vertical raindrop profile moving downward. The movement will appear clearly if the images capture the raindrop front. However, the actual process includes horizontal movement, raindrop development (growth), evaporation back of raindrops (dissipation), and diffusion (spreading) [13-15]. Therefore, to estimate raindrop vertical time travel, it needs to evaluate more than one VCUT and CAPPI image.

The optical flow method is one of the nowcasting analyses that use a sequence of radar product images such as CAPPI or CMAX [4, 16, 17]. However, only a horizontal movement evaluation can apply this method. A study has

incorporated Doppler radar data and the relevant numerical model to enhance the optical flow method, and overcome its drawbacks, such as considering no growth and decay. Further development of nowcasting methods used the 3D numerical models [18, 19] with observed data assimilation [9, 10]. These methods solve equations governing the process and their variational equations [19]. A hybrid approach developed a method by taking advantage of the radar rainfall data and the numerical model of weather prediction (mesoscale model five – MM5) that deal with wind direction, humidity, etc.[20]. Wide-area weather forecast practices commonly applied those methods.

2.6 The correlation between successive images

In [21], a correlation between sequences of the vertically integrated liquid (VIL) contour detected the movement of storms. It also identified storm growth and decay. A method to generate velocity vector patterns used image filtering and correlation analysis to provide nowcasting [22]. Another method for short-term cloud forecast used a lag cross-correlation analysis [23]. The lag cross-correlation analysis used successive IR satellite images of the same scene. Methods called TREC and COTREC adopted image recognition techniques that correlate between successive images [24]. A study has compared a cross-correlation technique and a multiple-step-ahead forecast method by [25] to the method using linear extrapolation of the centroids of rainfall features. The result shows that the cross-correlation technique performs better in terms of a series of statistical parameters.

Cross-correlation analysis with varying time lag can indicate the similarity of the shapes of two time-series curves and approximate the phase shift or delay time between them. The cross-correlation formula, $cc_{(x,y)}$, with lag analysis is as follows.

$$cc_{(x,y)} = \frac{\sum_{i=1}^{n}(x_i - \bar{x})(y_{i-k} - \bar{y})}{\sqrt{\sum_{i=1}^{n}(x_i - \bar{x})^2}\sqrt{\sum_{i=1}^{n}(y_{i-k} - \bar{y})^2}} \quad (2)$$

where x_i is the i^{st} first data series, y_i is the i^{st} second data series, $\bar{x}$ and $\bar{y}$ are the averaged values of the first and second data series, respectively, n is the number of data in a series, and k is the lag (Δt k is time lag).

3. RESULT AND DISCUSSION

3.1 Evaluation of interpolation methods

An algorithm for transforming PPI data to a 3D grid has been developed under Phyton interpreter [26], which covers NN and IDW interpolation methods for approximating R values at 3D grid nodes.

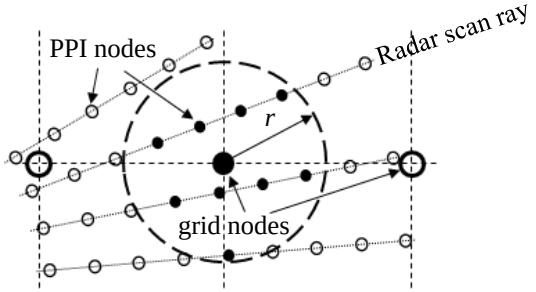

Fig. 4 Interpolation to a grid node (uses only values on the PPI nodes in solid black colour, r is the limiting distance)

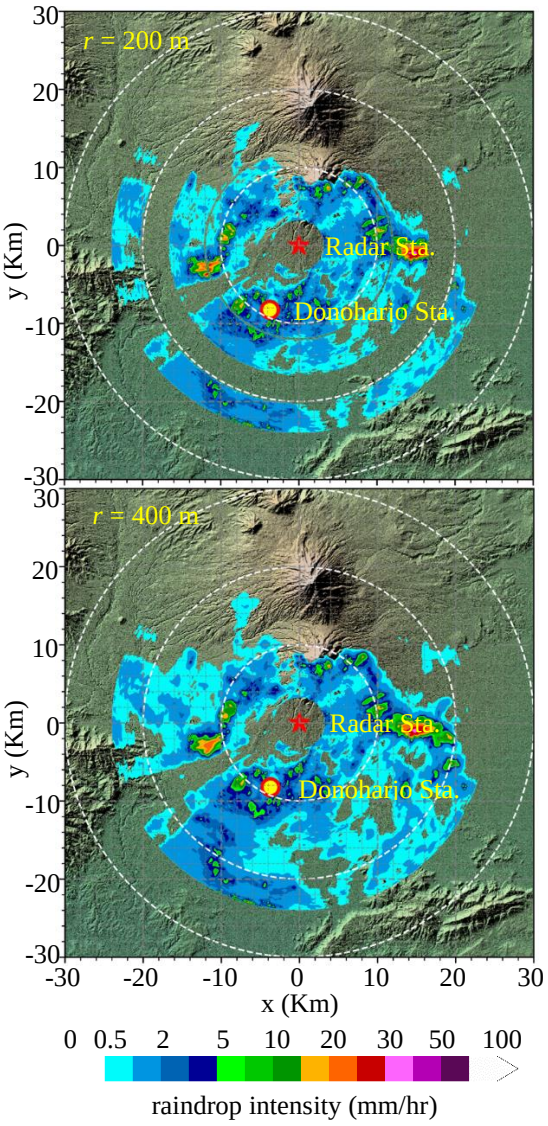

Fig. 5 The CAPPI contour at 2.0 Km on 19-02-2020 14:40:00 constructed from 100x100x100 m grid with r = 200 m (top) that produces a ring-shaped

gap and r = 400 m (bottom) (modified from [26])

The IDW interpolation method uses data on the neighbouring PPI nodes whose distance to a grid node less than a selected limit as shown in Fig. 4. As for the NN method, the value on the nearest PPI node is used.

Problems arose when the limiting distance, r, is too small or too big. A grid node may not have any PPI neighbouring node if r is too small. In a such condition, the value of that grid node is set to zero. If the value of r is too big, the neighbouring PPI nodes whose distance less than r become too many. The interpolation process uses a maximum number of 100 nearest neighbouring PPI nodes.

In applying the IDW method, after using several trial values on a 100x100x100 m grid, the optimal r was found to be 400. The power constant, p, was set to 3 as suggested by [27]. Fig. 5 shows a comparison of using r values of 200 m and 400 m. The top picture shows a ring shape gap of zero grid node values. Note that the colour scale applies to all other figures.

A CAPPI contour data can be converted to .kml format and displayed on the Google Earth oblique satellite view as shown in Fig. 6. The developed application can display CAPPI and VCUT, as shown in Fig. 7.

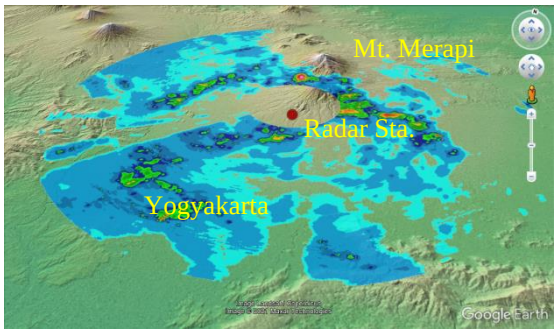

Fig. 6 The CAPPI contour is presented on Google Earth (modified from [26])

Fig. 9 depicts the comparison of using the IDW and NN interpolation methods. The IDW method with r equals 400 m provides a smoother contour than that provided by the NN method, however, the process takes a longer time.

A comparison between the use of the vertical grid intervals of 500 m and that of 100 m has evaluated the use of VCUT images for visual observation of the vertical movement of raindrops. The result in Fig. 8 shows that the 100 m grid captures significant many more features.

3.2 Correlation analysis

A cross-correlation analysis can assist to know how well the use of the raindrop intensity data at several Kilometer above the ground for estimating the additional time of a flood warning time. This analysis evaluates pairs of data whose locations above the Donoharjo ARR Station (UTM: 432811.83, 9149845.00; 400 m above m.s.l.) [28]. Fig. 10 shows raindrop intensity data series of several elevations.

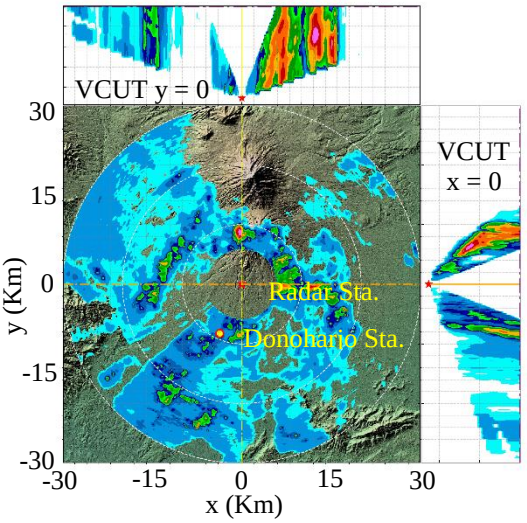

Fig. 7 Snap shoot of CAPPI 3.0 Km and VCUT contours showing heavy rainfall on the area 10 Km to the east and 8 Km to the north of Radar station [26]

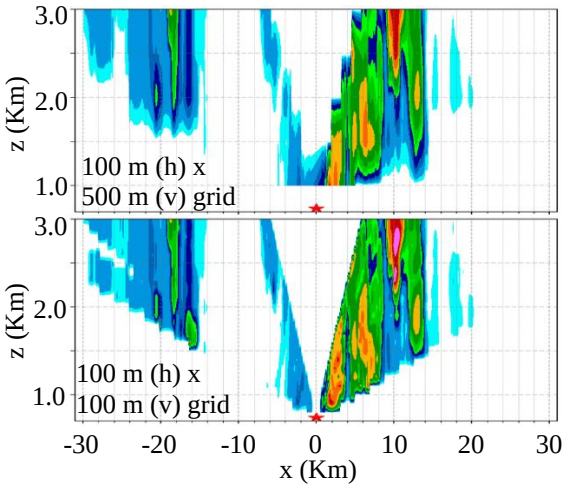

Fig. 8 VCUT contours of 500 m vertical interval grid (top) and 100 m vertical interval grid (bottom) [26]

There is a high intensity of raindrops captured between 13:16 and 13:36. The appearance of time lag of the peak intensities among data of different elevations does not exist. However, their values vary, and the highest values are at 1300 m and 1500 m. The lowest value is at 3000 m. A second captured peak of raindrops intensity is 13.45 mm/hr. That peak is at 2500 m, and also does not show any

time lag with time-series data of the other elevation. The third one has a 24.95 mm/hr peak at 3000 m, and this case shows a 2-minute time lag for the data at 1500 m and 1300 m.

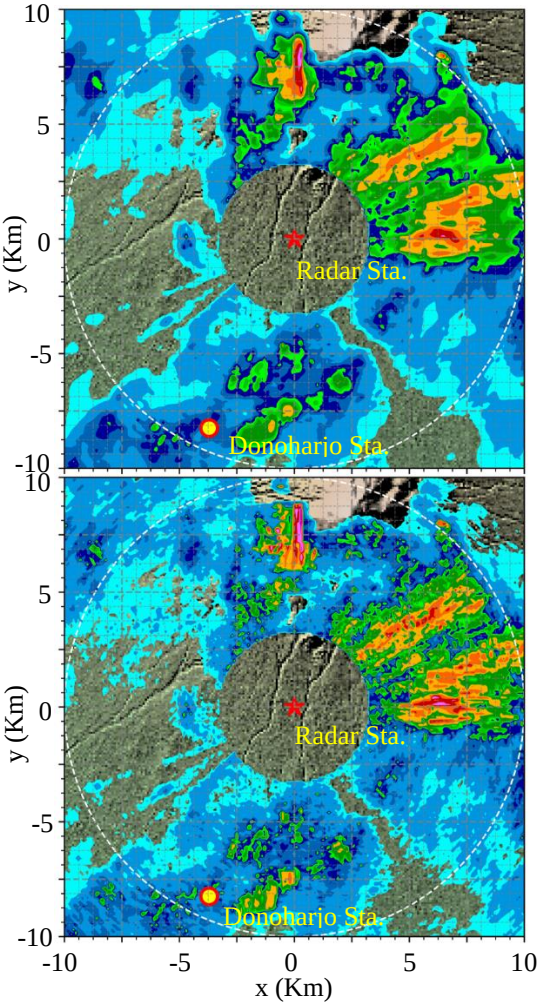

Fig. 9 The result of CAPPI 2.0 Km contours of the 19-02-2020 14:30 data created using IDW (top) and NN (bottom) interpolation methods [26]

The fourth one has a 9.07 mm/hr peak at 2500 m. Again, time lags appear showing the raindrops recorded at 3000 m came first, and 4 minutes later the raindrops at 2500 m were recorded, and 6 minutes later the raindrops at 1500 m and 1300 m were recorded with little different intensity. This different characteristic shows that there are different processes in those four rainfall events.

A sequence of CAPPI contour images shows that within the above period of rainfall, a wind drift appeared. See Fig. 11. Based on the presence of a weak wind drift heading southeast, a series of cross-correlation analysis between time series of raindrop intensity at elevation 1300 m (about 900 m above Donoharjo Sta.) and at elevation 3000 m above Donoharjo Sta. and other locations with 100 m zig-zag offset heading northwest as shown in Fig. 12.

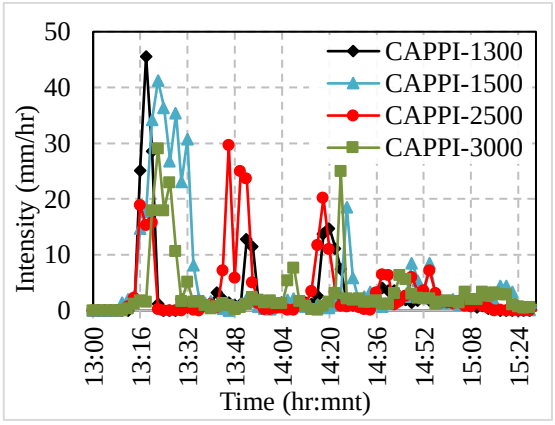

Fig. 10 Time series data of raindrop intensity above Donoharjo Sta at CAPPI 1300, 1500, 2500, 3000 m in 19-02-2020 from 13:00 to 15:30

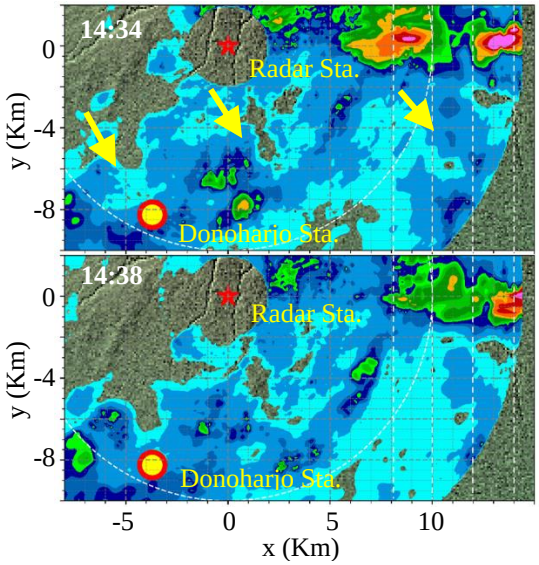

Fig. 11 Successive contour images of CAPPI 1.5 Km showing decaying rain drop intensity and a weak wind drift heading southeast

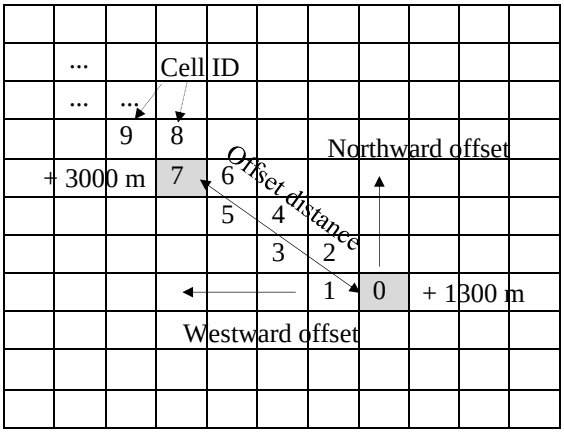

Fig. 12 The offset locations of analyzed data at an elevation of 3000 m from that of 1300 m

The results show that the maximum cross-correlation coefficient value is 0.785. This occurs at time-series data pair whose 400 m offset westward and 300 m offset northward (500 m horizontal distance) with a 4-minute time lag (see Fig. 13). The maximum cross-correlation coefficient of the pair of time-series data without location offset is 0.625 with the same 4-minute time lag. The maximum cross-correlation coefficient values drop from 0.693 to 0.365 as the offset distance increasing from 566 m to 1487 m. The above analysis results show that, based on the cross-correlation analysis, the estimated travel time for raindrops to travel from elevation of 3000 m to 1300 m is approximately 4 minutes. There is still a 900 m distance to reach the ground. By applying a linear extrapolation, it needs about 6 minutes for raindrops to travel from elevation 3000 m to reach the ground. Therefore, the additional time for flood warning time is about 6 minutes.

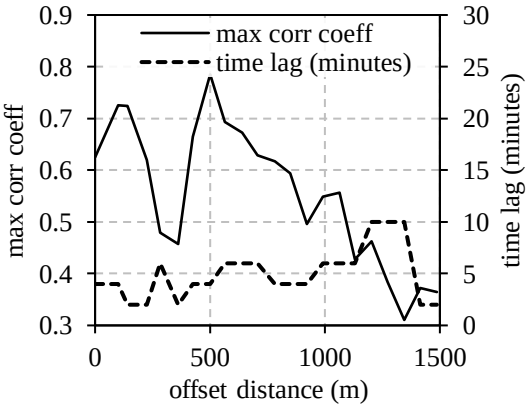

Fig. 13 The maximum cross-correlation coefficient and time lag vs offset distance of the +3000 m and +1300 m data series

4. CONCLUSION

The study has shown that the interpolation of PPI data of the X-Band MP Radar into a 3D grid gives the best performance when using the IDW method with a 100x100x100 m grid size, the limit searching distance value of 400 m, and power value of 3. The use of the data on the grid for cross-correlation analysis, for the case of rainfall in 19-02-2020 at the ARR Donoharjo Station (+400 m), gives an estimated additional flood warning time of 6 minutes.

This method needs the knowledge of wind drift direction on the area that can be indicated from successive CAPPI contour images. Wind drift direction may also be indicated by evaluating the maximum cross-correlation coefficient of all 360^o offset locations surrounding the lowest grid node above the ground station under evaluation.

5. ACKNOWLEDGEMENT

The author would like to thank the SATREPS Project, which provides rainfall radar. Many thanks also to be addressed to all colleagues who maintain the rainfall radar works. This research received a grant scheme from the Civil and Environmental Engineering Department, Eng. Faculty, UGM.

6. REFERENCES

[1] Sujono J., Jayadi R., and Nurrochman F., Heavy Rainfall Characteristics at South-West of Mt. Merapi- Yogyakarta and Central Java Province, Indonesia, Int. J. of Geomate, Vol. 14, Issue 45, 2018, pp. 184–191.

[2] Hambali R., Legono D., Jayadi R., and Oishi S., Improving Spatial Rainfall Estimates at Mt. Merapi Area Using Radar-Rain Gauge Conditional Merging, J. Disaster Res., vol. 14, no. 1, 2019, pp. 69–79.

[3] Hambali R., Legono D., and Jayadi R., Correcting Radar Rainfall Estimates Based on Ground Elevation Function, J. Civ. Eng. Forum, vol. 5, 2019, pp. 301–310.

[4] Hambali R., Legono D., and Jayadi R., The Application of Pyramid Lucas-Kanade Optical Flow Method for Tracking Rain Motion using High-resolution Radar Images, J. Teknol., vol. 83, no. 1, 2020, pp. 105–115.

[5] Syarifuddin M., Oishi S., Legono D., Hapsari R.I., and Iguchi M., Integrating X-MP radar data to estimate rainfall-induced debris flow in the Merapi volcanic area, Adv. Water Resour., vol. 110, 2017, pp. 249–262.

[6] Furuno Electric Co. Ltd., Install. Man. SSE-14-0023_17, Compact Dual Polarimetric X-Band Doppler Weather Model WR-2100, 2018, pp 1-101.

[7] Paski J.A.I., Permana D.S., Hastuti M.I., and Sudewi R.S.S., Dampak Asimilasi Data Radar Produk Cappi pada Prediksi Kejadian Hujan Lebat di Jabodetabek Menggunakan Model WRF-3DVAR (Impact of Cappi Product Radar Data Assimilation on Heavy Rain Prediction in Jabodetabek Using the WRF-3DVAR Model), J. Meteorol. dan Geofis., vol. 20, no. 1, 2019, pp. 47–54.

[8] Rahma N.A., Verdyansyah A., Faza M.Z., Nugraheni I.R., and Deranadyan G., Identifikasi Arah Sebaran dan Ketinggian Erupsi Gunung Berapi Menggunakan Citra Radar Cuaca (Identification of the Distribution Direction and Height of Volcanic Eruption Using Weather Radar Images), GEOMATIKA, vol. 26, no.2, 2020, pp. 71–82.

[9] Otsuka S., Tuerhong, G., Kikuchi R., Kitano Y., Taniguchi Y., Ruiz J.J. Satoh S., Ushio T.,

and Miyoshi T., Precipitation Nowcasting with Three-Dimensional Space-Time Extrapolation of Dense and Frequent Phased-Array Weather Radar Observations, Weather Forecast., vol. 31, no. 1, 2016, pp. 329–340.

[10] Heistermann M., Jacobi S., and Pfaff T., Technical Note: An open-source library for processing weather radar data (WRADLIB), Hydrol. Earth Syst. Sci., vol. 17, no. 2, 2013, pp. 863–871.

[11] North K.W., Oue M., Kollias P., Giangrande S.E., Collis S.M., and Potvin C.K., Vertical air motion retrievals in deep convective clouds using the ARM scanning radar network in Oklahoma during MC3E, Atmos. Meas. Tech., vol. 10, no. 8, 2017, pp. 2785–2806.

[12] Wilson J.W. and Mueller C.K., Nowcasts of thunderstorm initiation and evolution, Weather Forecast., vol. 8, no. 1, 1993, pp. 113–131.

[13] Bechini R. and Chandrasekar V., An enhanced optical flow technique for radar nowcasting of precipitation and winds, J. Atmos. Ocean. Technol., vol. 34, no. 12, 2017, pp. 2637–2658.

[14] Bowler N.E.H., Pierce C.E., and Seed A., Development of a precipitation nowcasting algorithm based upon optical flow techniques, J. Hydrol., vol. 288, no. 1–2, 2004, pp. 74–91.

[15] Woo W. and Wong W., Operational application of optical flow techniques to radar-based rainfall nowcasting, Atmosphere (Basel), vol. 8, no. 3, 2017, p. 48.

[16] Sun J., Xue M., Wilson J.W., Zawadzki I., Ballard S.P., Onvlee-Hooimeyer J., Joe P., Barker, D.M., Li, P., and Golding B., Use of NWP for nowcasting convective precipitation: Recent progress and challenges, Bull. Am. Meteorol. Soc., vol. 95, no. 3, 2014, pp. 409–426.

[17] Baldauf M., and Wetterdienst D., The COSMO model: towards cloud-resolving NWP, Recent Developments in Numerical Methods for Atmosphere and Ocean Modelling-Proceedings of a Seminar, 2014, pp. 107–122.

[18] Kim Y., Maki M., and Lee D.-I., Data that effectively demonstrate the benefits of a 3D CAPPI algorithm, Data Br., vol. 25, 2019, p. 104-116.

[19] Tsai C.-C., Yang S.-C., and Liou Y.-C., Improving quantitative precipitation nowcasting with a local ensemble transform Kalman filter radar data assimilation system: Observing system simulation experiments, Tellus: A Dyn. Meteorol. Oceanogr., vol. 66, no. 1, 2014, p. 1-16 (21804).

[20] Cano C.A.M., Using a hybrid approach to improve rainfall prediction for water management. Unesco-IHE, 2009.

[21] Evans J.E. and Ducot E.R., Corridor integrated weather system, Lincoln Lab. J., vol. 16, no. 1, 2006, p. 59.

[22] Van Horne M.P., Short-term precipitation nowcasting for composite radar rainfall fields, Massachusetts Institute of Technology, 2003.

[23] Hamill T.M. and Nehrkorn T., A short-term cloud forecast scheme using cross-correlations, Weather Forecast., vol. 8, no. 4, 1993, pp. 401–411.

[24] Mecklenburg S., Joss J., and Schmid W., Improving the nowcasting of precipitation in an Alpine region with an enhanced radar echo tracking algorithm, J. Hydrol., vol. 239, no. 1–4, 2000, pp. 46–68.

[25] Baltas E. and Mimikou M., Short‐term rainfall forecasting using radar data, Int. J. Water Resour. Dev., vol. 10, no. 1, 1994, pp. 67–77.

[26] Syahmi M.A., Pengembangan Aplikasi Pembaca Data Hujan Radar X-Band MP Gunung Merapi (Development of Application Software for X-Band MP Radar Data Reader for Mt. Merapi Area), Final Project Report, Civil and Environmental Eng. Dept., UGM, Yogyakarta, 2021.

[27] Livneh B. and Rajagopalan B., Development of a gridded meteorological dataset over Java island, Indonesia 1985–2014, Sci. data, vol. 4, no. 1, 2017, pp. 1–10.

[28] Hambali R., Legono D., and Jayadi R., Analisis Keandalan Data Penakar Hujan Otomatis Sebagai Acuan Koreksi Perkiraan Hujan Radar (Analysis of the Reliability of Automatic Rainfall Measurement Data as a Reference for Correction of Estimated Rainfall Radar), J. Tek. Pengair. J. Water Resour. Eng., vol. 10, no. 2, 2019, pp. 151–159.